PAPER

Shifts in valence states in bimetallic MXenes revealed by electron energy-loss spectroscopy (EELS)

To cite this article: Alexandre C Foucher et al 2022 2D Mater. 9 025004

View the article online for updates and enhancements.

You may also like

- Exploring MXene-based materials for nextgeneration rechargeable batteries Yuanji Wu, Yingjuan Sun, Jiefeng Zheng et al
- Harnessing the unique properties of MXenes for advanced rechargeable batteries

Deobrat Singh, Vivekanand Shukla, Nabil Khossossi et al.

- Physical properties of 2D MXenes: from a theoretical perspective

Aurélie Champagne and Jean-Christophe Charlier

2D Materials



RECEIVED

4 December 2021

REVISED 4 January 2022

4 January 2022

ACCEPTED FOR PUBLICATION
13 January 2022

PUBLISHED
31 January 2022

PAPER

Shifts in valence states in bimetallic MXenes revealed by electron energy-loss spectroscopy (EELS)

Alexandre C Foucher¹, Meikang Han², Christopher E Shuck², Kathleen Maleski², Yury Gogotsi² and Eric A Stach^{1,*}

- Department of Materials Science and Engineering and Laboratory for Research on the Structure of Matter, University of Pennsylvania, Philadelphia, PA, 19104, United States of America
- A J Drexel Nanomaterials Institute and Department of Materials Science and Engineering, Drexel University, Philadelphia, PA 19104, United States of America
- * Author to whom any correspondence should be addressed.

E-mail: stach@seas.upenn.edu

Keywords: MXenes, bimetallic structures, STEM-EELS, valence state

Supplementary material for this article is available online

Abstract

MXenes are an emergent class of two-dimensional materials with a very wide spectrum of promising applications. The synthesis of multiple MXenes, specifically solid-solution MXenes, allows fine tuning of their properties, expands their range of applications, and leads to enhanced performance. The functionality of solid-solution MXenes is closely related to the valence state of their constituents: transition metals, oxygen, carbon, and nitrogen. However, the impact of changes in the oxidation state of elements in MXenes is not well understood. In this work, three interrelated solid-solution MXene systems (Ti_{2-y}Nb_yCT_x, Nb_{2-y}V_yCT_x, and Ti_{2-y}V_yCT_x) were investigated with scanning transmission electron microscopy and electron energy-loss spectroscopy to determine the localized valence states of metals at the nanoscale. The analysis demonstrates changes in the electronic configuration of V upon modification of the overall composition and within individual MXene flakes. These shifts of oxidation state can explain the nonlinear optical and electronic features of solid-solution MXenes. Vanadium appears to be particularly sensitive to modification of the valence state, while titanium maintains the same oxidation state in Ti–Nb and Ti–V MXenes, regardless of stoichiometry. The study also explains Nb's influential role in the previously observed electronic properties in the Nb–V and Nb–Ti systems.

1. Introduction

Two-dimensional (2D) transition metal carbides and nitrides (MXenes) were discovered in 2011 when $Ti_3C_2T_x$ (T_x represents the surface groups, -O, -OH, -F, etc) was successfully produced by selective etching of Al from Ti_3AlC_2 [1]. MXenes have the general formula $M_{n+1}X_nT_x$, where M is an early transition metal (Ti, Nb, V, etc), X is C and/or N, and n = 1-4 [1, 2]. This class of materials has been widely studied due to their desirable optical [3], electronic [4], and mechanical properties [5], coupled with their ease of synthesis and processing from aqueous suspensions [6], their scalable synthesis [7], and their use of earth-abundant elements in their composition that potentially allow low-cost manufacturing

[8]. MXenes are also explored for use in electrochemical energy storage [9], additives for composites, biomedicine, and many other applications [10].

Recently, double transition metal MXenes have been synthesized. A few examples include $Mo_2Ti_2C_3T_x$ [11], $Cr_2TiC_2T_x$ [12], $Mo_4VC_4T_x$ [2], $Ti_{2-y}Nb_yCT_x$, $Ti_{2-y}V_yCT_x$, $V_{2-y}Nb_yCT_x$ (y is between 0 and 2) [13], along with many others [11, 14]. In some cases, such as $Mo_2Ti_2C_3T_x$ and $Cr_2TiC_2T_x$ [12], the structures have thermodynamic ordering where the two elements are in different layers and do not intermix. In other cases, such as $Mo_4VC_4T_x$ [2] or $Ti_{2-y}Nb_yCT_x$ [13], the elements are randomly distributed throughout all layers and intermix [15]. For solid-solution MXenes, control over the chemistry allows for tunability of the MXene

properties and improves their performance and stability.

For instance, $Ti_{2-y}Nb_yCT_x$ and $Nb_{2-y}V_yCT_x$ have been reported as tunable electromagnetic interference (EMI) shielding materials [16]. The Nb content of these solid-solution MXenes modulates the EMI shielding performance. Furthermore, $Ti_{2-\nu}Nb_{\nu}CT_{x}$ and $Nb_{2-\nu}V_{\nu}CT_{x}$ were shown as promising materials for electrochemical applications [17]. It was demonstrated that the composition determines the electrochemical capacitance and the stability of the material in an aqueous environment, with some mixed compositions outperforming the pure M MXenes. Finally, a combination of Mo_2CT_x with Co-doped MoS₂ has enhanced catalytic performance for the hydrogen evolution reaction (HER) [18]. These observations demonstrate the effect of combining two transition metals to modify the electronic configuration at the surface of materials in order to define and enhance chemical and physical properties [19, 20].

Hence, an extensive range of applications can be targeted by forming M-site solid solutions in MXenes. However, the origin of the changes in MXene properties due to alloying is not well understood. Changes in electronic and optical properties have been reported by changing the composition of $Ti_{2-\nu}Nb_{\nu}CT_{x}$, $Ti_{2-\nu}V_{\nu}CT_{x}$, and $V_{2-\nu}Nb_{\nu}CT_{x}$, with differing trends for each [13]. For instance, an optical absorption peak was observed when the Nb content was increased in $Ti_{2-y}Nb_yCT_x$. Similarly, the resistivity of Ti_{2-y}Nb_yCT_x increases with Nb concentration. Increased absorption in UV-vis spectra was observed between 400 nm and 700 nm for Ti_{1.6}Nb_{0.4}CT_x and between 300 nm and 450 nm for $V_{1.6}Nb_{0.4}CT_x$. Finally, the resistivity of $Ti_{2-\nu}V_{\nu}CT_x$ MXenes decreased with V concentration, except for $Ti_{1.6}V_{0.4}CT_x$. These observations indicate that the stoichiometry and ultimately the electronic configuration of transition metals in MXene crystals play a crucial role in determining their characteristics.

To elucidate the impact of valence states in solidsolution MXenes, a STEM-EELS analysis was performed to investigate the electronic structure of these transition metals at the nanoscale. The electronic configuration of oxygen and carbon were also studied, and EELS maps were collected to determine the spatial distribution of elements at the atomic scale. EELS is particularly suitable for light elements and transition metals (O, N, C, Ti, V). For these elements, the signal-to-noise ratio is very high, allowing to identify the edges' shape and position and determine the valence state configuration. More importantly, STEM-EELS can generate maps of the samples showing compositional and valence state data at the atomic scale. Thus, it is possible to locally identify shifts in oxidation state that will determine the physical and chemical properties of the material. This is impossible

with other bulk approaches such as x-ray photoelectron spectroscopy (XPS) or x-ray absorption spectroscopy.

2. Experimental methods

2.1. Materials

To synthesize the MAX phase precursors, Ti (99.5%, -325 mesh, Alfa Aesar), Al (99.5%, -325 mesh, Alfa Aesar), Nb (99.99%, -325 mesh, Beantown Chemical), V (99.5%, -325 mesh, Alfa Aesar), and graphite (99%, -325 mesh, Alfa Aesar) powders were used. To topochemically synthesize the MXenes from their respective MAX phase: hydrochloric acid (HCl, 36.5%–38%, Fisher Chemical), hydrofluoric acid (HF, 48.5%–51%, Acros Organics), lithium fluoride (LiF, 98.5%, Alfa Aesar), and tetramethylammonium hydroxide (TMAOH, 25 wt%, Acros Organics).

2.1.1. MAX phase synthesis

For each mixture, a $M_1:M_2:Al:C$ ratio of 2 - y:y: 1.1:0.9 was mixed, where y is 0.4, 0.8, 1.2, or 1.6, and M is Nb, Ti, and/or V. The respective precursor powders were mixed with 10 mm zirconia balls in a 2:1 ball/powder weight ratio. The mixture was first placed into plastic jars and then ball milled at 60 rpm for 18 h. The powder mixture was transferred into alumina crucibles, which were placed into a hightemperature furnace (Carbolite Gero). Ar was continually flown through the furnace (200 CCM) for 1 h prior to heating during synthesis. For all samples, the heating and cooling rate was 3 $^{\circ}$ C min⁻¹. The furnace was heated to 1550 °C for 2 h. After cooling, the samples were milled using a TiN-coated milling bit, then were sieved to less than 75 μ m. The powders were then washed in 9 M HCl overnight to remove residual intermetallics.

2.1.2. Synthesis of $Ti_{2-v}Nb_vCT_x$

For the synthesis of MXenes, it is important to follow all proper safety protocols [21]. $Ti_{2-y}Nb_yCT_x$ (y=0.4, 0.8, 1.2, and 1.6) was synthesized by selectively etching the corresponding $Ti_{2-y}Nb_yAlC$ powders with LiF and HCl. Typically, 1 g of $Ti_{2-y}Nb_yAlC$ powder was added to an etchant solution of LiF (1.5 g), HCl (15 ml), and deionized (DI) water (5 ml), and stirred for 48 h at 35 °C. Afterward, the solution was washed by centrifugation at 3500 rpm for 2 min. This washing process was repeated until pH > 6. Finally, the delaminated $Ti_{2-y}Nb_yCT_x$ was attained by centrifuging the swelled sediment at 7500 rpm for 3 min.

2.1.3. Synthesis of $Nb_{2-y}V_yCT_x$ and $Ti_{2-y}V_yCT_x$ $Nb_{2-y}V_yCT_x$ and $Ti_{2-y}V_yCT_x$ were synthesized by selectively etching the corresponding $Nb_{2-y}V_yAlC$ and $Ti_{2-y}V_yAlC$ MAX phases with HF. Typically, 1 g of $Nb_{2-y}V_yAlC$ was added to 20 ml HF (50 wt%)

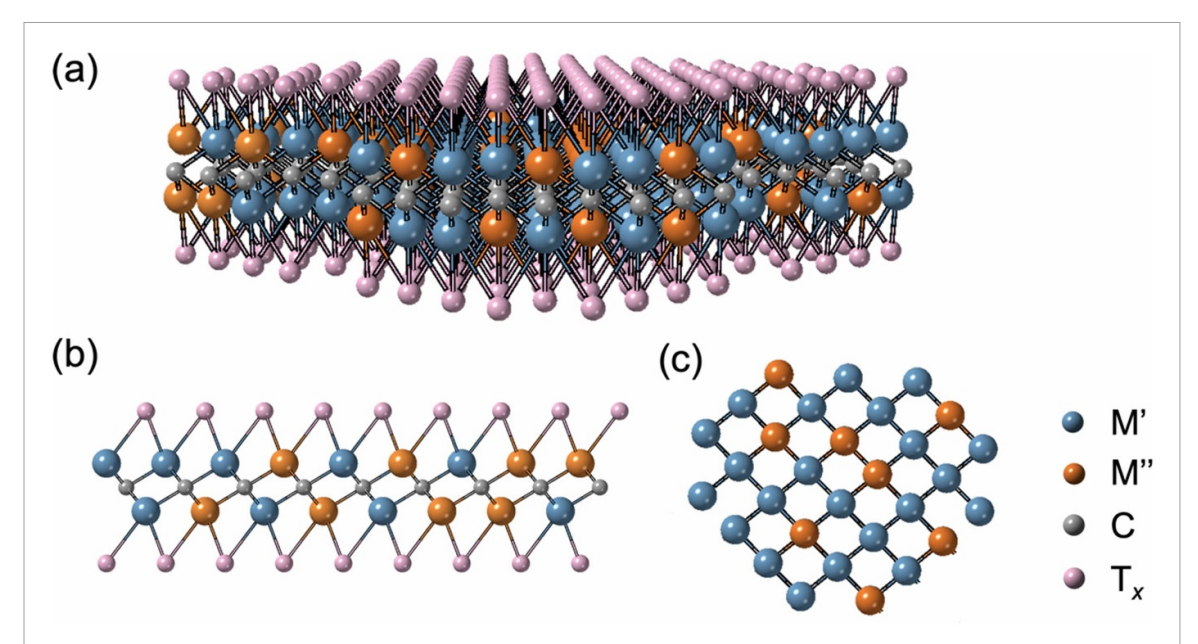


Figure 1. Schematics summarizing the structure of bimetallic MXenes with two transition metals M' and M''. (a) Side view of MXene flake. (b) Slice of the previous figure showing the two metallic rows. (c) Top view of a typical bimetallic MXene showing the random alloying of metals M' and M''. T_x represents the surface group, -O, -OH, -F, etc.

and stirred for 48 h at 35 °C. Afterward, the solution was washed with DI water by centrifugation until pH > 6. After washing, the sediment was mixed with 0.5 g of TMAOH in 20 ml of DI water and stirred for 12 h at room temperature. Finally, the mixture was washed with centrifugation at 10 000 rpm for 10 min. This washing procedure was repeated until pH < 8. The Nb_{2-y}V_yCT_x colloidal solution was collected by centrifugation at 3500 rpm for 10 min. The synthesis procedure of Ti_{2-y}V_yCT_x was the same as Nb_{2-y}V_yCT_x, except the etching time was 24 h. Schematics of the synthesized bimetallic MXenes are provided in figure 1.

2.2. Transmission electron microscopy

Images and energy dispersive x-ray spectroscopy (EDS) data were collected with a JEOL NEOARM instrument operated at 200 kV in scanning transmission electron microscopy (STEM) mode. The sample was first ground and diluted in isopropanol. A drop of the solution was then deposited on lacey carbon films supported on copper grids (Electron Microscopy Science). For imaging and EDS analysis, the probe current was 150 pA, the condenser lens aperture was 40 μ m, and the camera length was 4 cm. Two JEOL EDS detectors above the sample collected the fluorescent x-rays. The images were acquired with Digital-Micrograph, a software provided by Gatan Inc. For electron energy-loss spectroscopy (EELS), the same probe current and condenser lens aperture was used as for EDS, except that the camera length was 2 cm. A Gatan imaging filter entrance aperture of 5 mm was used, and the EELS data were obtained with a K2-IS camera.

3. Results and discussion

EELS maps of $Ti_{1.6}V_{0.4}CT_x$, $Ti_{1.2}V_{0.8}CT_x$, $Ti_{0.8}V_{1.2}$ CTx, and Ti_{0.4}V_{1.6}CTx were collected and revealed no significant segregation of V or Ti around edges or defects. Instead, the maps show that a fully random solution has been achieved at the nanoscale (figure 2). We investigated regions in the MXenes with defects to check if the segregation of elements around holes and pits could explain the observed changes in the optical and electronic properties. No particular features or abnormalities could be detected when we compared Ti-Nb, Ti-V and Nb-V MXenes (figures S1 and S2 available online at stacks.iop.org/2DM/9/025004/mmedia). Hence, it is possible to conclude that compositional heterogeneities are not the source of the shifts in the optical or electronic properties observed in these materials. Similar maps for the Nb-V and Ti-Nb systems are shown in figure S3, where Nb was detected with EDS. The $L_{2,3}$ edges for Nb are at 2465 eV and 2371 eV loss, respectively, which are too high for the strong signal necessary to obtain detailed EELS maps at the atomic scale. Additional details, including diffraction patterns of the Ti–V MXenes shown in figure 2, are provided in the supporting information (figure S4). Based on the diffraction patterns, it was not possible to detect changes in the crystal structure when the Ti:V ratio was changed. An investigation of the diffraction patterns of the Ti-Nb and Nb-V MXenes yielded the same conclusion.

It should also be noticed that the MXene flakes looked similar, independent of stoichiometry. 2D layers with Nb had fewer defects, such as holes and

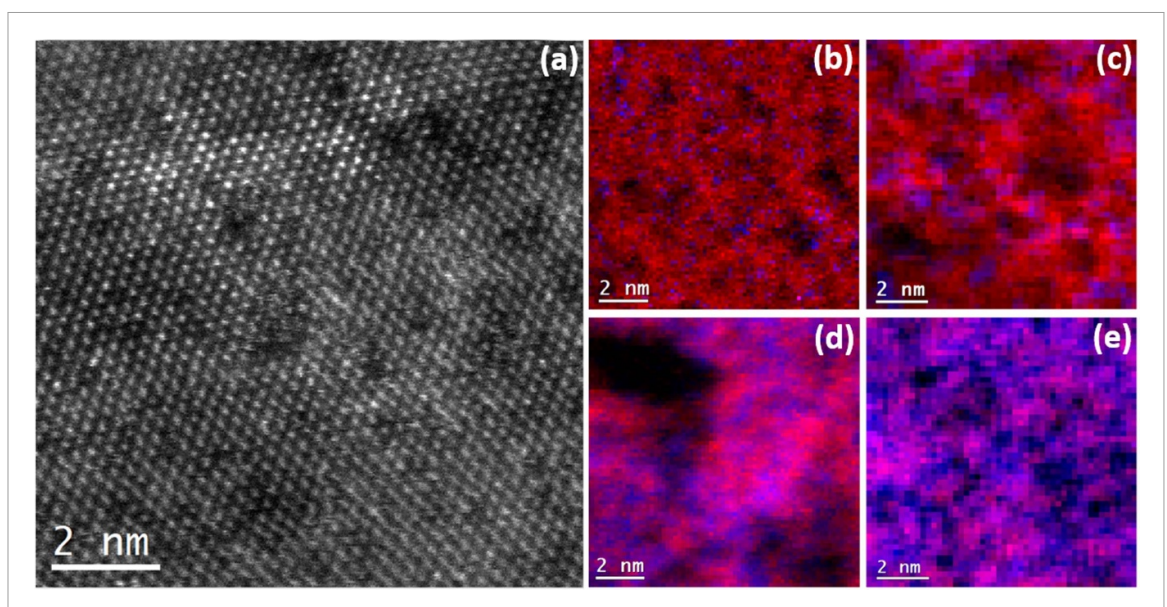


Figure 2. STEM-EELS investigation of Ti–V MXenes. (a) High-angle annular dark-field-STEM image of a $Ti_{1.6}V_{0.4}CT_x$ MXene showing common features observed in the flakes. The basal surface contains atomic-scale point defects and larger holes with a diameter up to 20 nm. (b) EELS map of $Ti_{1.6}V_{0.4}CT_x$ showing the uniform distribution of V and Ti, with no preferential segregation of transition metals around defects. V is in blue, and Ti is in red. (c) EELS map of $Ti_{1.2}V_{0.8}CT_x$. (d) EELS map of $Ti_{0.8}V_{1.2}CT_x$. (e) EELS map of $Ti_{0.4}V_{1.6}CT_x$. The stoichiometry does not change the uniform distribution of transition metals at the nanoscale. The corresponding STEM images to the EDS maps are provided in figure S5.

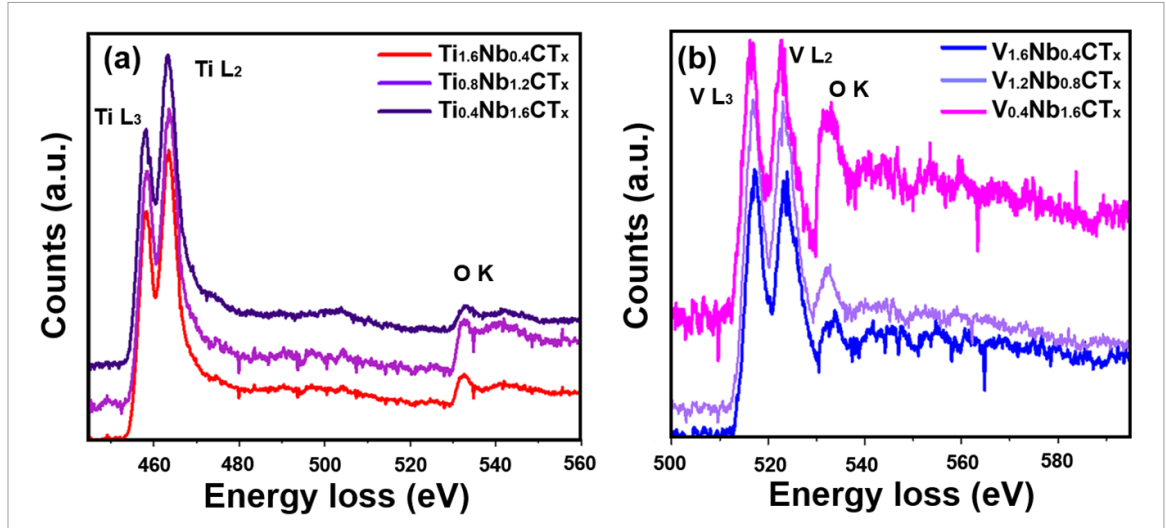


Figure 3. EELS spectra for Ti in Ti–Nb MXenes and V and O in Nb–V MXenes. (a) Ti $L_{2,3}$ for Ti_{1.6}Nb_{0.4}CT_x, Ti_{0.8}V_{1.2}CT_x, and Ti_{0.4}V_{1.6}CT_x. No substantial change of the Ti edges could be detected, indicating that changes to the Ti valence state are not responsible for changes in optical and electronic properties. (b) V $L_{2,3}$ edges and O K edge of V_{1.6}Nb_{0.4}CT_x, V_{1.2}Nb_{0.8}CT_x, and V_{0.4}Nb_{1.6}CT_x. The shape and ratios for the V $L_{2,3}$ edges do not change even though V_{1.6}Nb_{0.4}CT_x has different optical properties compared to the other MXenes in the Nb–V family.

atomic vacancies, but there was no substantial change when the ratios of transition metals were modified. This indicates that the morphology of MXene flakes cannot explain the difference in optical and electronic properties upon a shift in stoichiometry. It has also been shown that flake morphology and lateral dimensions do not affect optical properties of ${\rm Ti}_3{\rm C}_2{\rm T}_x$ as well [22]. Therefore, it is possible to conclude that the composition and potential modification of the electronic configuration is the origin of variations in physical and chemical properties.

The $L_{2,3}$ edges for V and Ti in Ti–V MXenes were then investigated. The ratio between the L_3 and L_2 edges is characteristic of the transition element valence states. Hence, a change of L_3/L_2 indicates a modification of the electronic configuration for either Ti or V. A typical series of EELS spectra for the Ti–V MXene family is shown in figure 3: Ti $L_{2,3}$ edges are located at 462 eV and 456 eV and the V $L_{2,3}$ edges are located at 521 eV and 513 eV. Additionally, the oxygen K edge was also collected at 532 eV loss. The results are summarized in figures 4(a) and (b). In

IOP Publishing 2D Mater. **9** (2022) 025004 A C Foucher et al

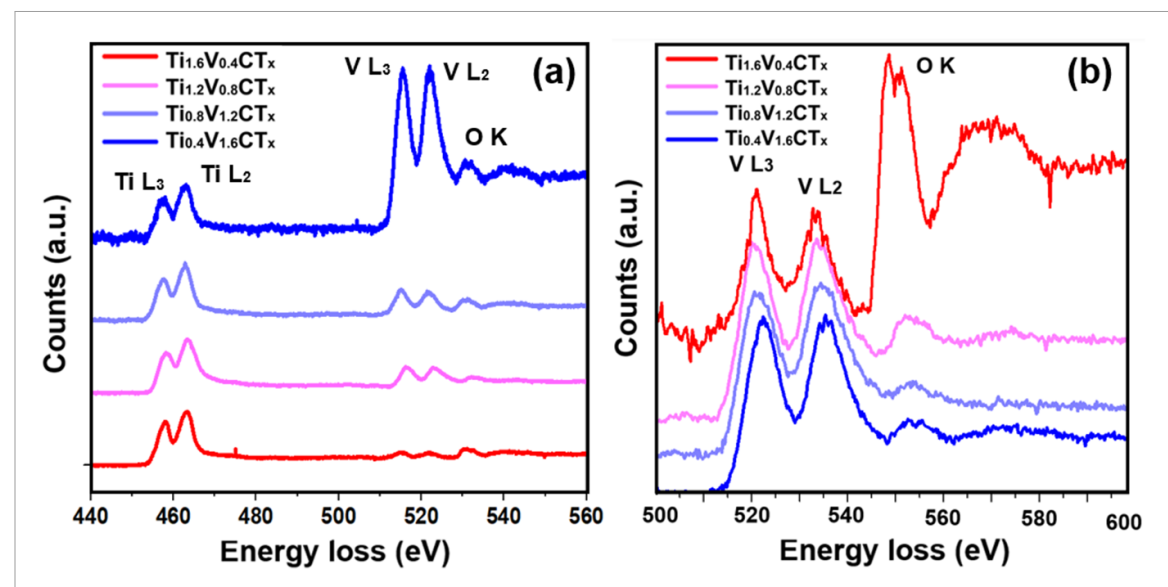


Figure 4. EELS spectra of the Ti $L_{2,3}$ and V $L_{2,3}$ edges. (a) Ti $L_{2,3}$ and V $L_{2,3}$ edges for four Ti–V MXenes. The spectra were normalized with respect to Ti L_3 . No substantial changes were observed in the Ti L_3/L_2 ratio, indicating no change in valence state. (b) V $L_{2,3}$ and O K EELS edges, with EELS spectra normalized with respect to V L_3 . A slight splitting of the O K edges is visible for the four MXenes, indicating that V has a high oxidation state [28].

figure 4(a), the height of the Ti L_3 edge has been normalized for the four considered stoichiometries to see changes in the Ti L_3 ratios. In figure 4(b), the four spectra have been normalized with respect to the V L_3 edge. The EELS spectra reveal no substantial Ti L_3/L_2 ratio variation or shift to higher energy losses for the EELS edges. In contrast, a slight V L_3/L_2 increase for Ti_{1.6}V_{0.4}CT_x was observed, compared to the other MXenes: Ti_{1.2}V_{0.8}CT_x, Ti_{0.8}V_{1.2}CT_x, and $Ti_{0.4}V_{1.6}CT_x$. To expand upon the results in figure 4, the L_3/L_2 ratios for Ti edges and V edges were measured for multiple regions in the four considered MXenes. The average ratios are provided in table 1, and at least five spectra were used for each MXene to obtain a representative average for the L_3/L_2 ratio. The standard deviation of all measurements did not exceed 0.03 for the L_3/L_2 ratio. It is clear that Ti is unaffected by the concentration of V in $Ti_{2-\nu}V_{\nu}CT_{x}$ MXenes, in contrast to V. Indeed, the increased V L_3/L_2 ratio correlates with the optical measurement in [13], where an absorption peak appears in the UV-vis spectrum between 400 nm and 700 nm. The increase of the L_3/L_2 ratio is due to a higher oxidation state of vanadium [23, 24]. Indeed, V(II) has L_3 and L_2 edges of similar height and hence appears to be the dominant species in $Ti_{1.2}V_{0.4}CT_x$, $Ti_{0.8}V_{1.2}CT_x$, and $Ti_{0.4}V_{1.6}CT_x$. This result is consistent with previous XPS studies on these materials [13]. In contrast, for $Ti_{1.6}V_{0.4}CT_x$, an L_3/L_2 ratio slightly above one, combined with a splitting of the oxygen K edge is consistent with V(III) [25]. Additionally, the presence of V(III) is correlated with an absorption peak between 400 nm and 700 nm, and is thus is in good agreement with the known optical properties of V₂O₃ [26]. It should be stressed that the presence of V(II) as a minority oxide is very unlikely, as it has never observed in V-based MXenes. The

Table 1. L_3/L_2 ratio for Ti and V in Ti–V MXenes. Ti_{1.6} V_{0.4}CT_x has a different V L_3/L_2 ratio compared to other MXenes. A higher V L_3/L_2 edges ratio indicates a higher oxidation state.

Ti–V MXene	Ti L_3/L_2 ratio	V L ₃ /L ₂ ratio
$Ti_{1.6}V_{0.4}CT_x$	0.8	1.09
$Ti_{1.2}V_{0.8}CT_x$	0.76	0.97
$Ti_{0.8}V_{1.2}CT_x$	0.77	1.02
$Ti_{0.4}V_{1.6}CT_x$	0.74	1.02

Table 2. Ti L_3/L_2 ratios for Ti–Nb MXenes and V L_3/L_2 ratios for V–Nb MXenes. The ratio does not change substantially with stoichiometry. For V–Nb MXenes, the absorption of wavelengths between 300 nm and 450 nm for V_{1.6}Nb_{0.4}CT_x is not correlated with shifts of the EELS edges or a change of L_3/L_2 ratio.

Ti–Nb MXene	Ti L_3/L_2 ratio
$\overline{\text{Ti}_{1.6}\text{Nb}_{0.4}\text{CT}_x}$	0.79
$Ti_{0.8}Nb_{1.2}CT_x$	0.78
$Ti_{0.4}Nb_{1.6}CT_x$	0.76
Ti_2CT_x (reference)	0.76
V–Nb MXene	V L ₃ /L ₂ ratio
$Nb_{1.6}V_{0.4}CT_x$	1
$Nb_{0.8}V_{1.2}CT_x$	1.03
$Nb_{0.4}V_{1.6}CT_x$	1
V_2CT_r (reference)	1

bonding of V atoms on the surface with O atoms is responsible for vanadium oxidation and yields higher oxidation levels. Finally, the resistivity measured for $Ti_{1.6}V_{0.4}CT_x$ was higher than $Ti_{1.2}V_{0.4}CT_x$. This seems to be due to the increased oxidation state of vanadium, as resistivity increases with the vanadium oxidation state [27].

The analysis was expanded to include V–Nb and Ti–Nb MXenes. Multiple regions were investigated, and the average ratios are provided in tables 2. This data shows an unchanged V L_3/L_2 ratio for V–Nb

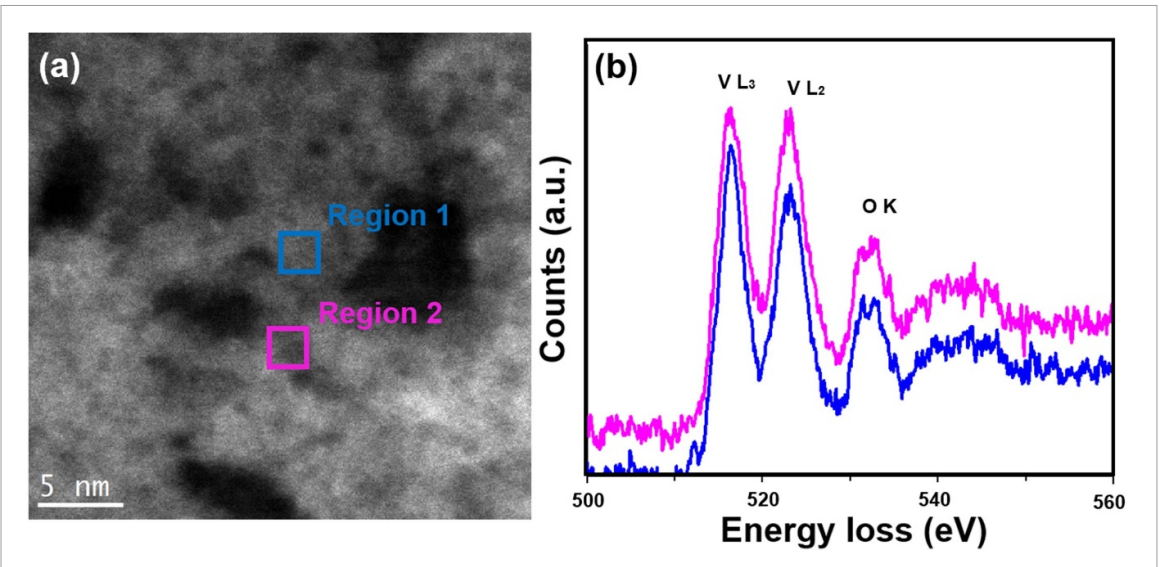


Figure 5. Image and corresponding EELS spectra of two surveyed regions in $Ti_{0.8}V_{1.2}CT_x$. The VL_3/L_2 ratio decreases from 1.16 to 1.01, indicating that region 1 is more oxidized than region 2. Thus, heterogeneities in the valence state can be induced to modify the properties of MXenes.

structures, and the same conclusion can be made for Ti L_3/L_2 for Ti-Nb MXenes. This indicates that the valence state of Ti does not play a crucial role in modifying the properties of Nb-based MXenes, even though Ti is more easily oxidized than Nb [29, 30]. For the Ti–Nb structure, the absorption peak height between 400 nm and 600 nm is incremental and appears directly correlated with the Nb concentration. This is different from the Ti-V MXenes, where an absorption peak could only be seen for $Ti_{1.6}V_{0.4}CT_x$ because of an increased oxidation state of vanadium. The substantial shift of the absorption spectrum observed for V_{1.6}Nb_{0.4}CT_x cannot be explained by the available EELS data for V-Nb structures. A potential explanation could be the presence of V(V) in V-rich MXenes. As shown in a previous publication, vanadium-based MXenes are easily oxidized, impacting the functionality of the 2D flakes [23, 31]. When V has the same valence state as V_2O_5 , the L_3/L_2 ratio is close to 0.97 and shows strong absorbance between 300 nm and 450 nm [26, 32]. This would reconcile the observed optical properties with the unchanged EELS data. It should be stressed that V₂O₅ might not be the only oxide present in $Nb_{0.4}V_{1.6}CT_x$. In contrast, based on previous work, V(II) is dominant in $Nb_{1.6}V_{0.4}CT_x$ and $Nb_{0.8}V_{1.2}CT_x$, and the presence of V(II) is consistent with the EELS and absorption data [13].

In summary, one can conclude that modification of the oxidation states of Ti is not the main reason for the changing Ti–Nb, indicating that Nb is primarily responsible for the changes in conductivity and optical properties. An increased resistivity was reported when the Nb concentration was higher in V–Nb and Ti–Nb MXenes. The increase of resistivity in each family indicates the particular role of Nb in tuning electrical properties. For V–Nb

MXenes, the presence of a strong absorption between 300 nm and 450 nm can be justified by the presence of V₂O₅, which does not contradict our EELS data. For Ti–V MXenes, V undergoes substantial changes in the electronic configuration as the high L_3/L_2 ratio in Ti_{1.6}V_{0.4}CT_x indicates that V is more oxidized in this specific sample. In contrast, the Ti $L_{2,3}$ edges remain unchanged as no shifts of edges or changes in the L_3/L_2 ratio were observed. This suggests that V will be primarily interacting with O atoms to oxidize and ultimately inhibit the oxidation of Ti atoms. Ti may remain unchanged in Ti-Nb MXenes because of the protective role of incorporating Nb into the 2D structures. It is consistent with previous reports indicating that Nb-doped MXenes are particularly stable materials [33].

Additionally, the properties of solid-solution MXenes can be impacted by local changes in the valence state of some transition elements. This has been primarily observed in V-based MXenes, where the oxidation state of V locally changes. Figure 5 shows two EELS spectra collected from small surveyed regions. The areas have a similar thickness and structure. These spectra indicate a significant change of the V L_3/L_2 ratio between region 1 and region 2. Since the V L_3/L_2 ratio is 1.16 for region 1 and 1.01 for region 2, we can conclude that region 1 is more oxidized. Region 1 likely contains V(III), whereas region 2 contain V(II). Based on the shape of the EELS edges and the optical measurements, a higher oxidation state for vanadium such as V(V)is unlikely. The multiple valence states in vandium have also been observed in other V-based structures, and the observed shifts are not necessarily correlated with defects [34]. Local heterogeneities and subtle modifications detected by EELS can lead to variations of mechanical, optical, and electronic properties.

Ultimately, control over these heterogeneities can tune the physical, in particular optical, properties of MXenes.

As an aside, basal planes and edges were also analyzed, and there was no substantial change of Ti $L_{2,3}$ edges when both were compared. Finally, carbon K edges were measured for the three families and consistently showed a π^*/σ^* equal to 0.55. This observation suggests that carbon plays a minor role in the local modification of the valence state or with MXenes with different stoichiometry. Finally, the presence of oxygen has a more significant impact. Indeed, the ratio between V L3 and O K edges is higher for region 1 than region 2. This is consistent with the above measurements of the L_3/L_2 ratio to determine the oxidation state. It also indicates that O primarily bonds with V and modifies its electronic configuration. Modulating the oxidation state at the nanoscale on MXenes can be beneficial to tune properties, especially since metal-oxide hybrid 2D materials are gaining interest [35]. This becomes especially important for the rational design of new 2D materials with complex chemistries, targeting specific properties or applications [36].

4. Conclusions

Herein, a STEM-EELS analysis revealed a correlation between the properties of solid-solution MXenes and the valence state of transition metals. The absorption peaks for Ti_{1.6}V_{0.4}CT_x and Nb_{0.4}V_{1.6}CT_x are linked to the higher oxidation state of V. In contrast, Ti remains unchanged when the stoichiometry is modified in Ti-V or Ti-Nb MXenes. For Ti-Nb, shifts in conductivity and peaks in absorption spectra are mainly attributed to the effect of Nb. This explains the gradual increase of an absorption peak between 400 nm and 600 nm for Ti-Nb MXenes and the gradual reduction of resistivity when the Nb content is decreased. Finally, local heterogeneities affecting the oxidation state of V have been observed and can potentially impact the properties of V-based solidsolution MXenes. The above STEM-EELS investigation can be applied to a wide range of novel 2D materials to understand their physical and optical properties at the nanoscale.

Data availability statement

All data that support the findings of this study are included within the article (and any supplementary files).

Acknowledgments

This work was supported as part of the Integrated Mesoscale Architectures for Sustainable Catalysis (IMASC), an Energy Frontier Research Center funded by the US Department of Energy, Office of Science, Basic Energy Sciences under Award #DE-SC0012573. Experiments were also carried out at the Singh Center for Nanotechnology at the University of Pennsylvania, supported by the National Science Foundation (NSF) National Nanotechnology Coordinated Infrastructure Program Grant NNCI-1542153. Additional support to the Nanoscale Characterization Facility at the Singh Center has been provided by the Laboratory for Research on the Structure of Matter (MRSEC) supported by the National Science Foundation (DMR-1720530). Development of solid-solution MXenes at Drexel University was supported by the National Science Foundation (DMR-2041050).

Conflict of interest

The authors declare no competing financial interest.

ORCID iDs

Alexandre C Foucher https://orcid.org/0000-0001-5042-4002

Meikang Han https://orcid.org/0000-0003-3309-988X

Christopher E Shuck https://orcid.org/0000-0002-1274-8484

Kathleen Maleski https://orcid.org/0000-0003-4032-7385

Yury Gogotsi https://orcid.org/0000-0001-9423-4032

Eric A Stach https://orcid.org/0000-0002-3366-2153

References

- [1] Naguib M, Kurtoglu M, Presser V, Lu J, Niu J, Heon M, Hultman L, Gogotsi Y and Barsoum M W 2011 Two-dimensional nanocrystals produced by exfoliation of Ti₃AlC₂ Adv. Mater. 23 4248–53
- [2] Deysher G et al 2019 Synthesis of Mo₄VAlC₄ MAX phase and two-dimensional Mo₄VC₄ MXene with five atomic layers of transition metals ACS Nano 14 204–17
- [3] Maleski K, Shuck C E, Fafarman A T, Gogotsi Y, Maleski K, Shuck C E, Gogotsi A Y J and Fafarman A T 2021 The broad chromatic range of two-dimensional transition metal carbides Adv. Opt. Mater. 9 2001563
- [4] Yang Y et al 2020 Distinguishing electronic contributions of surface and sub-surface transition metal atoms in Ti-based MXenes 2D Mater. 7 025015
- [5] Lipatov A, Lu H, Alhabeb M, Anasori B, Gruverman A, Gogotsi Y and Sinitskii A 2018 Elastic properties of 2D Ti₃C₂T_x MXene monolayers and bilayers Sci. Adv. 4 eaat0491
- [6] Maleski K, Mochalin V N and Gogotsi Y 2017 Dispersions of two-dimensional titanium carbide MXene in organic solvents Chem. Mater. 29 1632–40
- [7] Shuck C E, Sarycheva A, Anayee M, Levitt A, Zhu Y, Uzun S, Balitskiy V, Zahorodna V, Gogotsi O and Gogotsi Y 2020 Scalable synthesis of Ti₃C₂T_x MXene Adv. Eng. Mater. 22 1901241
- [8] Jolly S, Paranthaman M P and Naguib M 2021 Synthesis of ${\rm Ti_3C_2T_z}$ MXene from low-cost and environmentally friendly precursors *Mater. Today Adv.* **10** 100139

- [9] Anasori B, Lukatskaya M R and Gogotsi Y 2017 2D metal carbides and nitrides (MXenes) for energy storage *Nat. Rev. Mater.* 2 16098
- [10] Al-Hamadani Y A J, Jun B M, Yoon M, Taheri-Qazvini N, Snyder S A, Jang M, Heo J and Yoon Y 2020 Applications of MXene-based membranes in water purification: a review Chemosphere 254 126821
- [11] Pinto D, Anasori B, Avireddy H, Shuck C E, Hantanasirisakul K, Deysher G, Morante J R, Porzio W, Alshareef H N and Gogotsi Y 2020 Synthesis and electrochemical properties of 2D molybdenum vanadium carbides—solid solution MXenes J. Mater. Chem. A 8 8957–68
- [12] He J, Ding G, Zhong C, Li S, Li D and Zhang G 2018 Cr₂TiC₂-based double MXenes: novel 2D bipolar antiferromagnetic semiconductor with gate-controllable spin orientation toward antiferromagnetic spintronics Nanoscale 11 356–64
- [13] Han M et al 2020 Tailoring electronic and optical properties of MXenes through forming solid solutions J. Am. Chem. Soc. 142 19110–8
- [14] Nemani S K, Zhang B, Wyatt B C, Hood Z D, Manna S, Khaledialidusti R, Hong W, Sternberg M G, Sankaranarayanan S K R S and Anasori B 2021 High-entropy 2D carbide MXenes: TiVNbMoC₃ and TiVCrMoC₃ ACS Nano 15 12815–25
- [15] Shekhirev M, Shuck C E, Sarycheva A and Gogotsi Y 2021 Characterization of MXenes at every step, from their precursors to single flakes and assembled films *Prog. Mater.* Sci. 120 100757
- [16] Han M, Shuck C E, Rakhmanov R, Parchment D, Anasori B, Koo C M, Friedman G and Gogotsi Y 2020 Beyond Ti₃C₂T_x: MXenes for electromagnetic interference shielding ACS Nano 14 5008–16
- [17] Wang L, Han M, Shuck C E, Wang X and Gogotsi Y 2021 Adjustable electrochemical properties of solid-solution MXenes Nano Energy 88 106308
- [18] Bai J, Zhao B, Lin S, Li K, Zhou J, Dai J, Zhu X and Sun Y 2020 Construction of hierarchical V₄C₃-MXene/MoS₂/C nanohybrids for high rate lithium-ion batteries *Nanoscale* 12 1144–54
- [19] Lim K R G, Handoko A D, Johnson L R, Meng X, Lin M, Subramanian G S, Anasori B, Gogotsi Y, Vojvodic A and Seh Z W 2020 2H-MoS₂ on Mo₂CT_x MXene nanohybrid for efficient and durable electrocatalytic hydrogen evolution ACS Nano 14 16140–55
- [20] Bhat A, Anwer S, Bhat K S, Mohideen M I H, Liao K and Qurashi A 2021 Prospects challenges and stability of 2D MXenes for clean energy conversion and storage applications npj 2D Mater. Appl. 5 61
- [21] Shuck C E, Ventura-Martinez K, Goad A, Uzun S, Shekhirev M and Gogotsi Y 2021 Safe synthesis of MAX and MXene: guidelines to reduce risk during synthesis ACS Chem. Health Saf. 28 326–38
- [22] Maleski K, Ren C E, Zhao M Q, Anasori B and Gogotsi Y 2018 Size-dependent physical and electrochemical properties

- of two-dimensional MXene flakes *ACS Appl. Mater. Interfaces* **10** 24491–8
- [23] Venkatkarthick R, Rodthongkum N, Zhang X, Wang S, Pattananuwat P, Zhao Y, Liu R and Qin J 2020 Vanadium-based oxide on two-dimensional vanadium carbide MXene (V₂O_x@V₂CT_x) as cathode for rechargeable aqueous zinc-ion batteries ACS Appl. Energy Mater. 3 4677–89
- [24] Tan H, Verbeeck J, Abakumov A and van Tendeloo G 2012 Oxidation state and chemical shift investigation in transition metal oxides by EELS *Ultramicroscopy* 116 24–33
- [25] Laffont L, Wu M Y, Chevallier F, Poizot P, Morcrette M and Tarascon J M 2006 High resolution EELS of Cu–V oxides: application to batteries materials *Micron* 37 459–64
- [26] Choi N H, Kwon S and Kim H 2013 Analysis of the oxidation of the V(II) by dissolved oxygen using UV-visible spectrophotometry in a vanadium redox flow battery *J. Electrochem. Soc.* 160 A973–9
- [27] Pergament A L, Stefanovich G B, Kuldin N A and Velichko A A 2013 On the problem of metal-insulator transitions in vanadium oxides *ISRN Condens. Matter Phys.* 2013 960627
- [28] Gloskovskii A, Nepijko S A, Schönhense G, Therese H A, Reiber A, Kandpal H C, Fecher G H, Felser C, Tremel W and Klimenkov M 2007 Spectroscopic and microscopic study of vanadium oxide nanotubes J. Appl. Phys. 101 084301
- [29] Palisaitis J, Persson I, Halim J, Rosen J and Persson P O Å 2018 On the structural stability of MXene and the role of transition metal adatoms *Nanoscale* 10 10850–5
- [30] Echols I J, Holta D E, Kotasthane V S, Tan Z, Radovic M, Lutkenhaus J L and Green M J 2021 Oxidative stability of Nb_{n+1}C_nT_z MXenes J. Phys. Chem. C 125 18
- [31] Iqbal A, Hong J, Ko T Y and Koo C M 2021 Improving oxidation stability of 2D MXenes: synthesis, storage media, and conditions *Nano Converg.* 8 1–22
- [32] Kalavathi S, Selva V, Raju Q, Williams A, Fujiwara K, Hori T, Tanaka H, Ghiyasiyan-Arani M, Salavati-Niasari M and Fathollahi Zonouz A 2013 Valence state, hybridization and electronic band structure in the charge ordered AlV₂O₄ J. Phys.: Condens. Matter 26 015601
- [33] Fatima M, Fatheema J, Monir N B, Siddique A H, Khan B, Islam A, Akinwande D and Rizwan S 2020 Nb-doped MXene with enhanced energy storage capacity and stability Front. Chem. 8 168
- [34] Gustafsson J P 2019 Vanadium geochemistry in the biogeosphere–speciation, solid-solution interactions, and ecotoxicity Appl. Geochem. 102 1–25
- [35] Kumbhakar P et al 2021 Emerging 2D metal oxides and their applications Mater. Today 45 142–68
- [36] Wang Q, Velasco L, Breitung B and Presser V 2021 High-entropy energy materials in the age of big data: a critical guide to next-generation synthesis and applications Adv. Energy Mater. 11 2102355